

RESEARCH PAPER



Dual-target ligand discovery for Alzheimer's disease: triphenylphosphoranylidene derivatives as inhibitors of acetylcholinesterase and β -amyloid aggregation

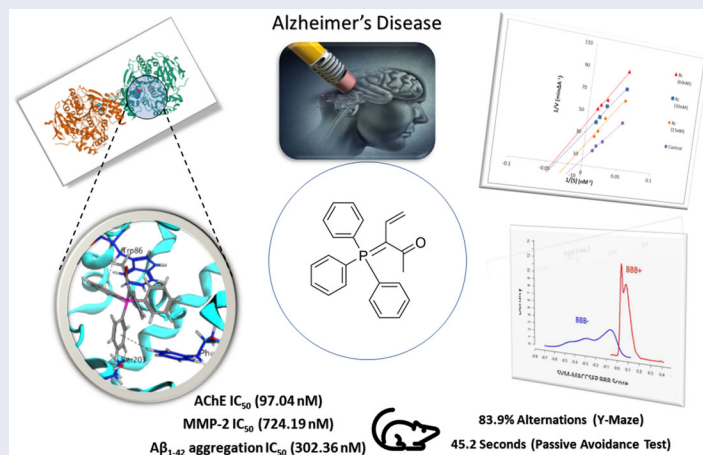
Marwa El-Hussieny^a, Mansoura A. Abd-El-Maksoud^a, Fouad M. Soliman^a, Marwa A. Fouad^{b,c} and Mohamed K. El-Ashrey^b

^aOrganometallic and Organometalloid Chemistry Department, National Research Centre, Giza, Egypt; ^bPharmaceutical Chemistry Department, Faculty of Pharmacy, Cairo University, Cairo, Egypt; ^cPharmaceutical Chemistry Department, School of Pharmacy, NewGiza University, Cairo, Egypt

ABSTRACT

Alzheimer disease (AD) is one of the major neurodegenerative diseases that could not be prevented or completely cured and may lead to death. Here, we target AChE and β -amyloid proteins. Synthesising new triphenylphosphoranylidene derivatives based on the surveyed literature and testing their biological activity revealed promising results especially for the acetyl triphenylphosphoranylidene derivative **8c**, which showed good inhibitor activity against AChE enzyme with IC_{50} in the nanomolar range (97.04 nM); on the other hand, it showed poor selectivity for AChE versus butyrylcholinesterase but with some futural structural modification, this selectivity can be improved. **8c** showed MMP-2 IC_{50} of 724.19 nM and $A\beta_{1-42}$ aggregation IC_{50} of 302.36 nM. A kinetic study demonstrated that compound **8c** uncompetitively inhibited AChE. Moreover, derivative **8c** showed low cytotoxicity, good *in vivo* behavioural studies including Y-maze and passive avoidance tests with activity similar to that of donepezil. Finally, *in silico* studies for **8c** predict its good penetration into BBB and good binding affinity in the AChE binding site.

GRAPHICAL ABSTRACT



ARTICLE HISTORY

Received 25 October 2022
Revised 15 December 2022
Accepted 3 January 2023

KEYWORDS





Triphenylphosphoranylidene; silane; acetylcholinesterase; β -amyloid; Alzheimer's disease


Introduction

Alzheimer disease (AD) is one of the neurodegenerative disorders that affects not only the patient but also the family and the caregiver¹. There are numerous theories that have been put forth to explain the causes, including the aggravation of ageing, the degeneration of cholinergic and cortico-cortical pathways, environmental factors like aluminium exposure, head injuries, malnutrition, mutations of the amyloid precursor protein (APP) and PSEN

genes, allelic variation in apolipoprotein E, mitochondrial dysfunction, immune system dysfunction, and infectious agents². AD is categorised as the third cause of death in the world after heart and cancer diseases and the affected people are expected to be more than ten million people by the next 30 years³.

Acetylcholinesterase (AChE) enzyme is the primary cholinesterase in the human body, it catalyses the hydrolysis of the neurotransmitters, acetylcholine (ACh) and other choline esters⁴. Each molecule of AChE hydrolyses about 25 000 of ACh per second

CONTACT Mohamed K. El-Ashrey  mohamed.elashrey@pharma.cu.edu.eg  Pharmaceutical Chemistry Department, Faculty of Pharmacy, Cairo University, P.O. 11562, Giza, Egypt; Marwa El-Hussieny  mrw_elhussieny@yahoo.com, me.awad@nrc.sci.eg  Organometallic and Organometalloid Chemistry Department, National Research Centre, 33 ElBohouth St., (Former El Tahrir), Dokki, P.O. 12622, Giza, Egypt

 Supplemental data for this article can be accessed online at <https://doi.org/10.1080/09553002.2022.2166040>.

© 2023 The Author(s). Published by Informa UK Limited, trading as Taylor & Francis Group.

This is an Open Access article distributed under the terms of the Creative Commons Attribution License (<http://creativecommons.org/licenses/by/4.0/>), which permits unrestricted use, distribution, and reproduction in any medium, provided the original work is properly cited.

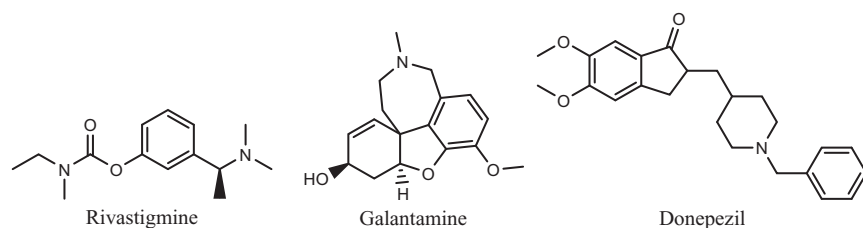


Figure 1. Examples of approved AChE inhibitors used for AD.

revealing its very high catalytic activity⁵. Drug or toxin that inhibits AChE leads to persistent high level of ACh within the synapses with increasing cholinergic activity. Irreversible AChE inhibitors are used as insecticides while reversible inhibitors are useful for several diseases such as Alzheimer's disease⁶. Many chemical derivatives showed good inhibitory activity against AChE^{7,8}, rivastigmine, galantamine, and donepezil are examples of approved AChE inhibitor drugs^{9–11} (Figure 1).

Butyrylcholinesterase (BuChE) is a non-specific cholinesterase enzyme that hydrolyses many choline-based esters and found mainly in blood plasma¹². Inhibition of BuChE in the periphery causes severe side effects such as the known AChE inhibitor Tacrine¹³. Also, this enzyme shows a compensatory effect in response to a greatly decreased AChE activity in the central nervous system (CNS) during AD progression¹⁴. So, it is valuable to make a selective AChE inhibitor ligand with minimum effect on the peripheral BuChE¹⁵.

On the other hand, amyloids are aggregates of proteins, where β -amyloids ($A\beta$) are the main components of amyloid plaques found in patients with AD^{16,17}. $A\beta$ are formed by the action of β - and γ -secretase enzymes on the precursor protein¹⁸. $A\beta$ molecules can aggregate to form some oligomers, which are toxic to nerve cells¹⁹. The other protein implicated in AD is the tau (τ) protein, which also forms misfolded oligomers²⁰. $A\beta_{1-40}$ and $A\beta_{1-42}$ are two isoforms of $A\beta$, $A\beta_{1-42}$ is less soluble and so more susceptible to aggregation²¹. It was also found that amyloid monomers interact with the peripheral active site (PAS) of AChE promoting the conformational changes that occur at amyloid proteins leading to an increase in their aggregation²². So, inhibiting the formation of $A\beta$ plaques is a powerful way to counteract the central degeneration that occurs in AD.

Moreover, matrix metalloproteinases (MMPs); which are present normally in low level and play an important role in tissue remodelling associated with various biological processes²³ are thought to degrade APP, which causes aggregation of $A\beta$. Additionally, it was noted that post-mortem brain tissue from AD patients had an enhanced expression of MMPs²⁴.

Based on the mentioned causes of AD, medicinal chemists are in a continuous journey to find a multitarget ligand that is able to; not only relieve the symptoms; but also slow down the progression of the disease²⁵. In the last decade, our research group has focussed on the synthesis of novel heterocyclic and homocyclic compounds, which have phosphorus moieties; these derivatives have industrial and biological importance^{26–31}.

There are numerous uses for organophosphorus chemicals in medicine for the treatment of AD, phosphonic acid derivatives were found to be extremely effective with an IC_{50} range of 0.01–0.2 μ M³². Along with the nonenzymatic conversion of Metriphosphate, a long-acting irreversible organophosphate AChE inhibitor, to the active ingredient Dichlorvos; (Figure 2), clinical trials were started to treat AD patients because of its capacity to improve cholinergic neurotransmission in the CNS. But, in a 6-months study on AD treatment, respiratory paralysis and problems with neuromuscular transmission were seen^{33,34}.

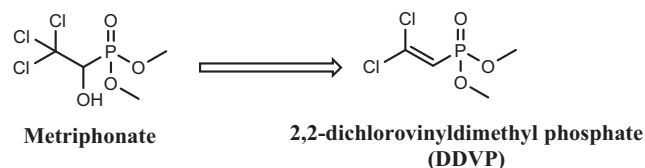


Figure 2. Non-enzymatic activation of metriphosphate.

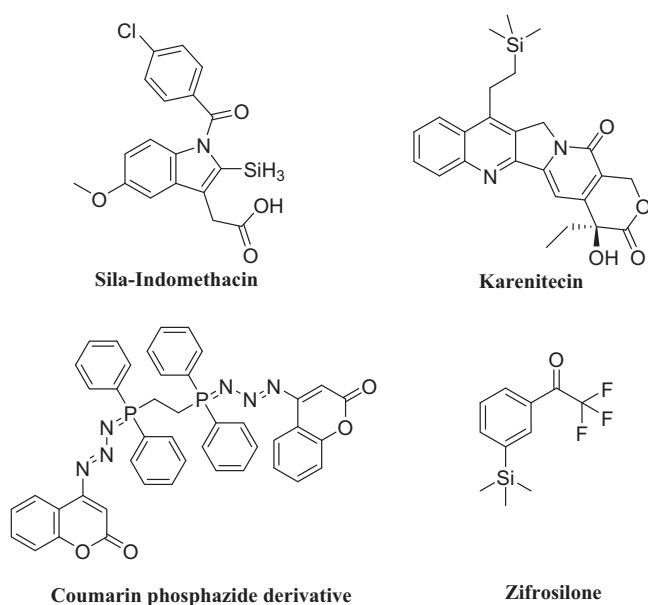


Figure 3. Reported silicone-containing compounds and coumarin phosphazide derivative.

Because silicon-containing molecules, such as those with methylsilyl, silanol, and silandiol groups, differ from those with carbon-carbon bases in terms of their chemical properties, organosilicon compounds have a variety of interesting applications, particularly in medicine as anti-inflammatory, antibacterial, and anticancer agents³⁵. Through the silyl group, silicon can be incorporated into organic molecules to offer them special features like enhancing lipophilicity, which promotes cell and tissue penetration and consequently increases potency and selectivity of organosilicon rather than carbon-based molecule³⁶. In addition, several medications have the silyl moiety, including the non-steroidal anti-inflammatory medicine, Sila-indomethacin³⁷ and the anticancer organosilicon drug, BNP-1350 (Karenitecin)³⁸. A silicon-containing compound called zifrosilone underwent clinical testing to treat Alzheimer's disease (Figure 3)³⁹.

Furthermore, we previously reported the discovery of a new coumarin phosphazide derivative as a selective and potent AChE and β -amyloid aggregation inhibitor⁴⁰. In conjunction with this work and based on the previous facts about the importance of phosphorus compounds as inhibitor for the Alzheimer's disease, we have synthesised some novel triphenylphosphoranylidenesilol-ylidene aniline, triphenylphosphoranylidenesilolone,

triphenylphosphoranylidenebutanoates, and cyclobutenes, as AChE inhibitors. Besides, the most potent compound was assessed for its AChE/BuChE selectivity, self-induced A β aggregation and MMP-2 inhibition ability. In addition, the most potent compound (**8c**) was studied for AChE inhibition kinetics. Moreover, it was studied for neuroblastoma toxicity and its ability to ameliorate scopolamine-induced cognitive impairment in rats. Then, it was subjected to a molecular docking simulation to establish its binding affinity and mode of action in the enzyme's binding site. Finally, drug-likeness prediction was utilised to analyse the pharmacokinetic properties.

Results and discussion

Chemistry

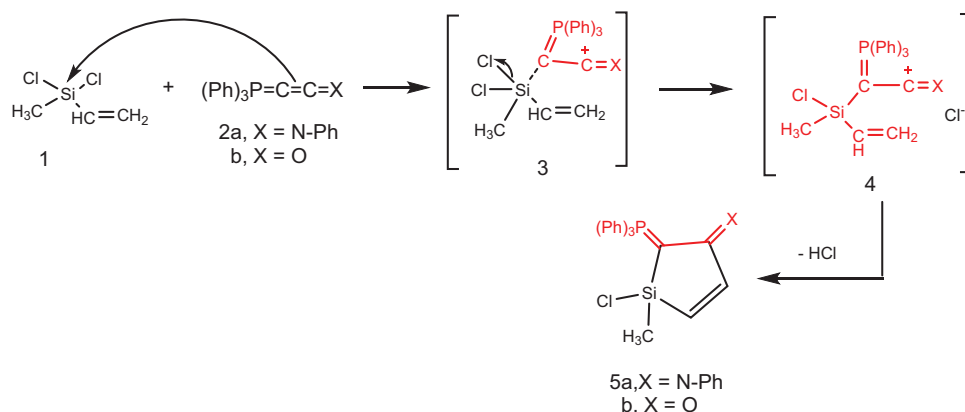
Reacting (N-phenyliminovinylidene)triphenylphosphorane (**2a**) with dichloromethylvinylsilane (**1**) in tetrahydrofuran (THF), afforded N-(1-chloro-1-methyl-2-((triphenylphosphoranylidene)methylene)-1H-silol-3(2H)-ylidene)aniline (**5a**). Chlorosilanes are generally recognised to be the most popular substrates for displacement reactions that produce high yields of substitution products, even with weak nucleophilic reagents under mild conditions⁴¹. So, it is believed that addition of the nucleophilic phosphacumulene (**2a**) to the vinyl silane (**1**) yields the intermediates (**3**) then (**4**). Cyclisation of the salt (**4**) afforded the phosphoranylidene silol ylidene aniline (**5a**). The structure of (**5a**) was substantiated by its spectral data. The ³¹P-NMR spectrum recorded a chemical shift for (**5a**) at δ 17.30 ppm. In the mass spectrum, the M⁺ appeared at 484. Reaction of (2-oxovinylidene)triphenylphosphorane (**2b**) with vinylsilane (**1**) afforded the corresponding 1-chloro-1-methyl-2-((triphenylphosphoranylidene)-1H-silol-3(2H)-one

(**5b**). Its ³¹P NMR spectrum showed a peak at δ 19.40 ppm and in its mass spectrum, the M⁺ appeared at 406 (Scheme 1).

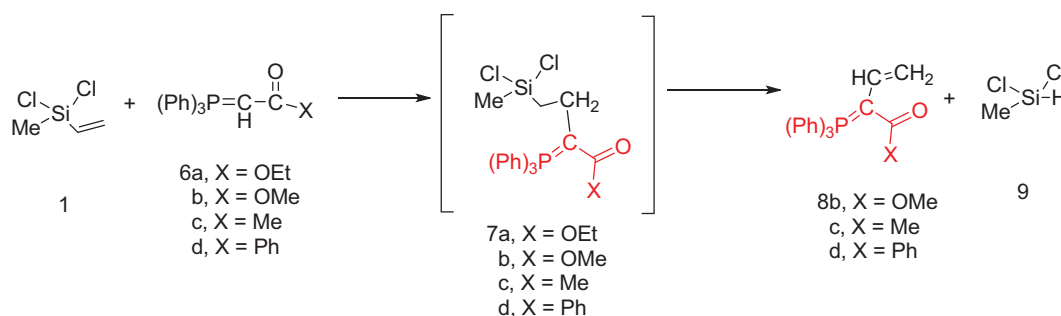
Next, the behaviour of the stabilised phosphonium ylides (**6a-d**) towards the vinylsilane (**1**) was also investigated in order to identify the place of the attack. It was found that, the ethoxycarbonyl-(**6a**), methoxycarbonyl-(**6b**), acetyl-(**6c**) or benzoyl-methylene triphenylphosphoranes (**6d**) reacted with vinylsilane (**1**) in THF yielding the phosphoranylidene butanoate derivatives (**7a-d**), which were isolated when the ethoxycarbonyl methylene triphenylphosphorane (**6a**) was used only. But in case of (**6b-d**), expulsion of the good leaving group dichloro(methyl)silane⁴² gave the corresponding triphenylphosphoranylidene derivatives (**8b-d**) by good yield. The structure of compound (**7a**) was established based on spectroscopic data. Also, the structure of compounds (**8b-d**) was elucidated on the basis and assignments of elemental and spectroscopic analysis such as in compound (**8d**), the ³¹P NMR spectrum shift was recorded at δ 21.66 ppm (Scheme 2).

Furthermore, we examined the reaction of 1,2-diphenylethylene (**10**) with the phosphacumulenes (**2a,b**). The reaction was carried out in boiling toluene in the presence of PdCl₂ affording the phosphoranylidene cyclobutene structures (**11a, 11b**), which were substantiated by their ³¹P NMR and MS spectral data. The ³¹P spectrum of (**11a**) revealed a signal at δ 22.25 ppm and in the MS, the m/z (%) appeared at 556 (M⁺). The ³¹P NMR spectrum of (**11b**) showed a signal at δ 33.94 ppm and the mass spectrum showed a molecular ion peak at m/z 481 (M⁺; Scheme 3).

On the other hand, by analogous procedure, N-[2,3-diethyl(triphenylphosphoranylidene)cyclobut-2-en-1-ylidene]aniline (**13a**) was obtained from the reaction of hex-3-yne (**12**) with the (N-phenyliminovinylidene)triphenylphosphorane (**2a**), in boiling toluene in the presence of PdCl₂. The ¹H NMR spectrum of (**13a**) showed signals at δ 1.75 (t, 3H, CH₃), 2.00 (q, 2H, CH₂) and its mass



Scheme 1. Synthesis of compounds 5(a & b) in THF.



Scheme 2. Synthesis of compounds 8 (a-c) in THF.

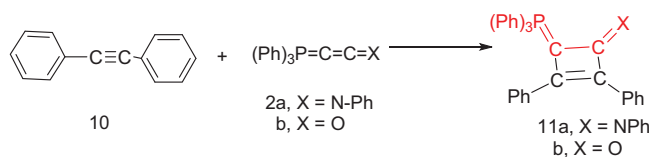
spectrum indicated the presence of the molecular ion peak at m/z 458 (M^+). Furthermore, the reaction of the hexyne (**12**) with the phosphacumulene (**2b**) was performed to give the phosphoranylidene cyclobutenone (**13b**). A signal at δ 28.31 was observed in its ^{31}P NMR spectrum (Scheme 4).

Finally, treatment of bis(trimethylsilyl)acetylene (**14**) with the phosphacumulene (**2b**) in refluxing toluene, afforded the corresponding 2,3-bis(trimethylsilyl)-4-(triphenylphosphoranylidene)cyclobut-2-enone (**15**) (Scheme 5).

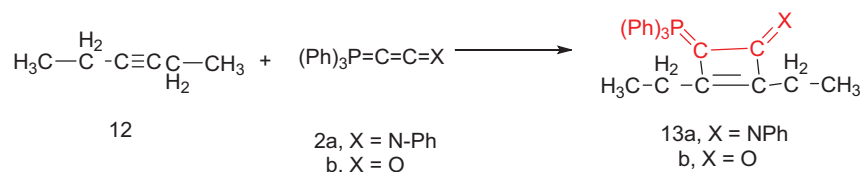
In vitro biological evaluation

In vitro AChE, BuChE, and MMP-2 inhibition assays

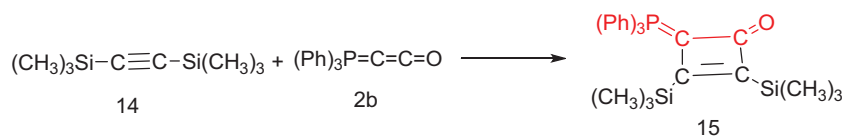
First, AChE inhibitory activity was tested for all the synthesised final compounds using the improved Ellman spectrophotometric method⁴³ and donepezil was used as the reference compound. The tested compounds showed IC_{50} values ranging from 97.04 to 508.03 nM compared to that of donepezil (34.42 nM; Table 1 and Figure 4). The triphenylphosphoranylidene silyl derivatives (**5a** and **5b**) showed relatively high IC_{50} values (206.25 and 345.04 nM, respectively), and it can be seen that replacing the aniline moiety in **5a** with carbonyl substitution as in compound **5b** causes a notable decrease in the AChE inhibitory activity. On the other hand, the other triphenylphosphoranylidene derivatives (**8c** and **8b**) have relatively low IC_{50} (97.04 and 157.78 nM, respectively) especially the acetyl derivative (**8c**). On the contrary, compound **8d** shows high IC_{50} (426.35 nM) indicating that benzoyl substitution dramatically decreases the inhibitory activity. Cyclobutene derivatives **11a** and **11b** showed extremely variable results as the aniline derivative (**11a**) showed a moderate inhibitory activity with IC_{50} of 184.73 nM while the oxo derivative (**11b**) showed the highest IC_{50} value among all the tested compounds (508.03 nM). Other cyclobutene derivatives with ethyl substitution (**13a** and **13b**) showed also variable results but on the contrary the oxo derivative (**13b**) revealed moderate activity (IC_{50} of 248.82 nM) while the aniline derivative (**13b**) showed high IC_{50} value of 507.05 nM. Finally, bis(trimethylsilyl)cyclobutenone derivative (**15**) has a good inhibitory activity with IC_{50} of 113.05 nM.



Scheme 3. Synthesis of compounds 11 (a & b) in the presence of PdCl_2 .



Scheme 4. Synthesis of compounds 13 (a & b) in boiling toluene in the presence of PdCl_2 .



Scheme 5. Synthesis of compound 15 in refluxing toluene.

Based on the obtained results, compound **8c** showing the highest activity against AChE enzyme was subjected for further investigation (Table 1).

In order to test the selectivity of the selected compound, the inhibitory activity of compound **8c** against BuChE enzyme was tested and compared to that of the reference compound, donepezil. This was carried out by using the modified Ellman spectrophotometric method. The results are summarised in (Table 2). As can be seen, compound **8c** did not show a remarkable selectivity for AChE enzyme more than BuChE and thus it can be considered as non-selective cholinesterase inhibitor.

Matrix Metalloproteinase-2 (MMP-2) is known for its impact on neurological disorders as AD⁴⁴⁻⁴⁶. Accordingly, compound **8c** was tested for MMP-2 inhibition and compared to imatinib as reference compound, but it showed IC_{50} of 724.19 nM, which is relatively higher than that for imatinib (328.76 nM) showing a weaker inhibition ability (Table 2).

Eventually, self-induced $A\beta_{1-42}$ aggregation was tested for **8c** derivative, which showed IC_{50} of 302.36 nM while the reference compound donepezil exhibited IC_{50} of 115.94 nM (Table 2).

From the above-mentioned results, it can be concluded that compound **8c** is a non-selective AChE/BuChE inhibitor with moderate activity against $A\beta_{1-42}$ aggregation and weak activity against MMP-2 enzyme.

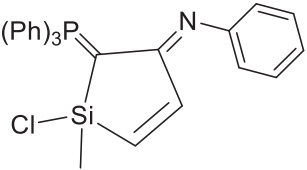
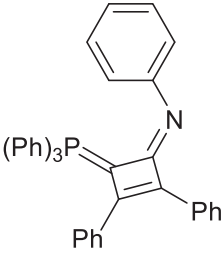
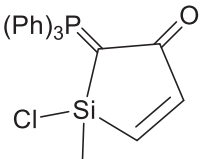
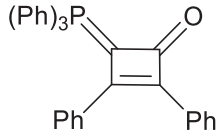
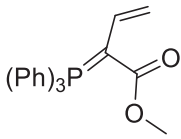
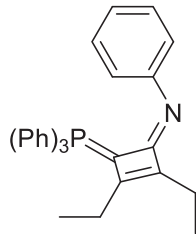
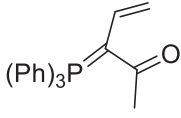
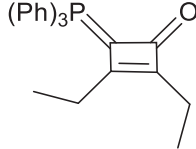
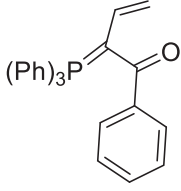
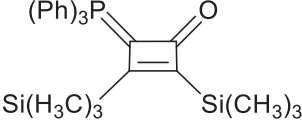
Kinetic study for AChE inhibition of compound 8c

To further understand the mechanism of AChE inhibition, the enzyme kinetics parameters of compound **8c**, the most effective AChE inhibitor, were examined. When the concentration of the inhibitor was increased, the Lineweaver-Burk double reciprocal plot ($1/V$ vs. $1/S$) revealed decreasing K_m and decreasing V_{max} values for both inhibited and uninhibited enzymes (Figure 5(a)). The Lineweaver-Burk plot and V_{max} and K_m patterns suggested an uncompetitive type of inhibition. Moreover, based on the Dixon plot with the K_i value as a negative intercept on the X-axis, the plot of the K_m versus different concentrations of **8c** produced an estimate of the inhibitory constant, K_i , of 15.7 nM (Figure 5(b)).

SH-SY5Y neuroblastoma cell toxicity of compound 8c

The safety of compound **8c** was assessed by testing its cytotoxicity effect on human neuroblastoma cell line SH-SY5Y. The cell viability was determined through using MTT assay. Compound **8c** showed a low cytotoxicity with CC_{50} value of $7.31 \pm 0.26 \mu\text{M}$ with high AChE inhibition activity ($\text{IC}_{50} = 97.04$ nM) and so, resulting in

Table 1. IC₅₀ values of the tested compounds and the reference drug donepezil against AChE enzyme.

| Compound | IC ₅₀ (nM) ^a ± SD | Compound | IC ₅₀ (nM) ^a ± SD |
|---|---|--|---|
|  | 206.25 ± 7.33 |  | 184.73 ± 9.22 |
| 5a | | 11a | |
|  | 345.04 ± 12.3 |  | 508.03 ± 16.5 |
| 5b | | 11b | |
|  | 157.78 ± 4.28 |  | 507.05 ± 22.1 |
| 8b | | 13a | |
|  | 97.04 ± 2.93 |  | 248.82 ± 10.4 |
| 8c | | 13b | |
|  | 426.35 ± 21.5 |  | 113.05 ± 4.82 |
| 8d | | 15 | |
| Donepezil | | | 34.42 ± 1.39 |

^aAverage of triplicate determination.

a high selectivity index (SI, CC₅₀ (nM)/IC₅₀(nM)) of 75.33, proving its safety on normal cell lines (Figure 6).

Behavioural studies

The most important criterion for assessing anti-AD medication candidates is cognitive improvement. Compound **8c**'s investigation in AD animal models was driven by promising *in vitro* results. In order to test potential anticholinergic medication candidates, the *in vivo* scopolamine model was employed to cause memory

impairment in mice. Scopolamine can inhibit the cholinergic system by antagonising the muscarinic receptor⁴⁷. Then, using donepezil as a positive control, the effects of compound **8c** on cognitive improvement were assessed using Y-Maze and passive avoidance tests.

Y-maze test

Animal working memory is assessed using the hippocampal-dependent Y-maze test. Working memory is measured using the spontaneous alternation score⁴⁸. Figure 7 demonstrates that the

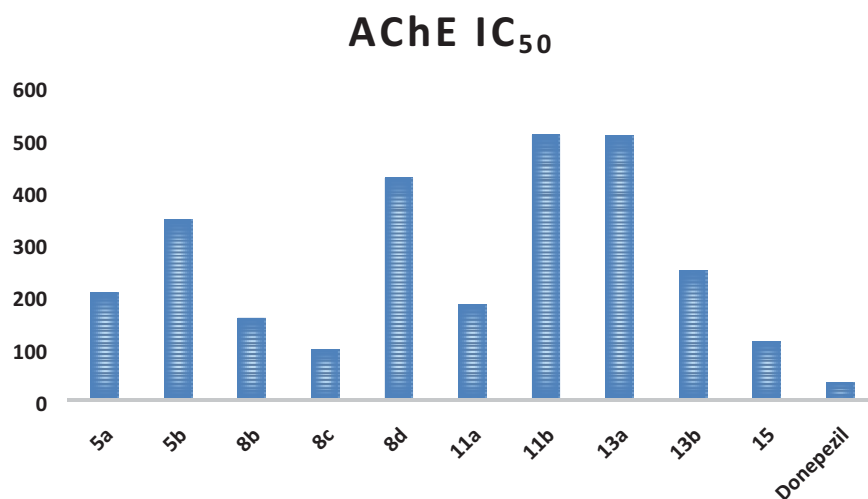


Figure 4. AChE IC_{50} of the tested compounds compared to that of donepezil.

Table 2. BuChE IC_{50} , selectivity index, MMP-2 IC_{50} , and self-induced $A\beta_{1-42}$ aggregation IC_{50} .

| Compound | BuChE IC_{50} (nM) \pm SD | Selectivity index | MMP-2 IC_{50} (nM) \pm SD | Self-induced $A\beta_{1-42}$ aggregation IC_{50} (nM) \pm SD |
|-----------|-------------------------------|-------------------|-------------------------------|--|
| 8c | 84.83 \pm 2.91 | 0.87 | 724.19 \pm 16.5 | 302.36 \pm 11.41 |
| Donepezil | 66.47 \pm 2.51 | 1.93 | – | 115.94 \pm 3.87 |
| Imatinib | – | – | 328.76 \pm 12.1 | – |

Selectivity index = (BuChE IC_{50})/(AChE IC_{50}).

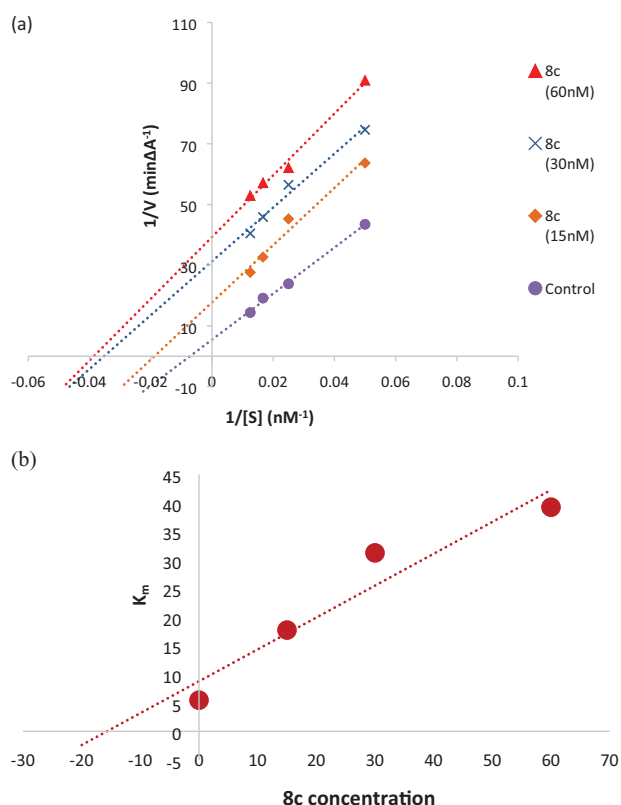


Figure 5. (a) Kinetic study on the mechanism of AChE inhibition by compound **8c**, Overlaid Lineweaver-Burk reciprocal plots of AChE initial velocity at increasing substrate concentration (15–60 nM) in the absence and in the presence of different concentrations of **8c**. (b) Dixon plot of compound **8c** showing the K_i value as negative intercept on the X-axis.

proportion of alternations was considerably lower in the scopolamine model group than in the control group (percent alternations = 51.2 and 82.1, respectively, at $p=0.01$). At a dose of

1 mg/kg for each, the mice group treated with compound **8c** demonstrated an increase in the percent alternations (percent alternations = 83.9 ($*p=0.01$)) that is non-significantly different from the increase in the donepezil-treated group (percent alternations = 80.7 ($*p=0.01$)), but this increase in the percentage of alternations was significantly different to the percentage of the model group.

Passive avoidance test

The central cholinergic neurons have a role in passive avoidance learning, while the hippocampus is principally in charge of controlling the learning response⁴⁹. The step-down passive avoidance test was used to assess compound **8c**'s ability to guard against memory loss. Figure 8 shows that the transfer latency time (TLT) of the scopolamine-treated group was substantially shorter than that of the control group (27.2 s, at $*p=0.01$). Comparable to donepezil at a dose of 1 mg/kg for each, treatment with compound **8c** (TLT = 45.2 s) demonstrated a substantial increase in TLT compared to the model group ($*p=0.01$). These *in vivo* results demonstrated that compound **8c** could cross the blood-brain barrier (BBB), hence enhancing scopolamine-induced cognitive impairment.

In silico studies

In silico prediction of BBB permeability of compound **8c**

Drugs that target the CNS must first cross the BBB. The inability of therapeutic molecules to penetrate the BBB is a key obstacle for CNS drug candidates and needs to be addressed quickly in the drug development process. Predicting BBB permeability of new CNS drugs is therefore crucial⁵⁰. Two webservers were used to predict the BBB permeability, pkCSM⁵¹ and SwissADME⁵². Both servers confirm that compound **8c** can penetrate BBB and this facilitates its action inside the CNS for treating AD (Figures 9 and 10).

Molecular docking

The molecular docking analysis was conducted using the X-ray crystallographic structure of human AChE in contact with (-)-galantamine, which was downloaded from protein data bank (PDB) (ID: 4EY6)⁵³. The protein structure of human BuChE in complex with its co-crystallized ligand from PDB ID; 7AIY⁵⁴.

The co-crystallized ligand (galantamine) was re-docked into the same binding site as part of the validation stage in order to confirm the tested compounds' actual binding mechanism. The binding energy result for galantamine was -14.99 kcal/mol. The validity of the docking process is demonstrated by the RMSD value of 0.78. An aromatic gorge, catalytic triad (CT), PAS, omega loop (OL), oxyanion hole (OH), anionic subsite (AS), and acyl binding pocket are some of the key regions of the AChE active site. Ser203, His447, and Glu334 make up the CT side, while Gly120, Ala204, and Gly121 make up the OH side. Finally, AS has Gly448, Glu202, Ile451, Tyr133, and Trp86. PAS has residues at Trp286, Tyr124, Asp74, Ser125, Tyr341, and Tyr337⁵⁵.

Compound **8c** showed a good binding score (-14.81 kcal/mol) compared to that of donepezil (-15.23 kcal/mol); the reference AChE inhibitor. **8c** derivative with three phenyl substitutions could bind through Arene-H interaction with Trp86 (AS), Gly121 (OH site), and Phe338 residues. Moreover, **8c** binds through arene-arene interaction with Tyr337 (PAS) and non-classical hydrogen bond with Ser203 (CT). On the other hand, donepezil showed hydrogen bond interaction with Tyr337 (PAS) through its carbonyl

oxygen in addition to arene interactions with Tyr341 (PAS) and Trp286 (AS), Figures 11 and 12.

On the other hand, compound **8c** showed good binding energy score with BuChE active site (-10.24 kcal/mol) with hydrogen bonding with Thr120, Phe329, and His438 amino acid residues (Figure 13). So, it was clear from the docking study that compound **8c** showed good binding affinity to AChE and BuChE enzymes, which confirms its good biological activity against both enzymes.

Conclusion

Searching for new chemical compounds that target one of the major neurodegenerative diseases; AD; is always a major concern for chemistry researchers. Focussing on phospharylidene derivatives which had been proved to have good anti-Alzheimer activity and synthesising ten new derivatives in a hope to find a good candidate for AD. Biological evaluation of the synthesised derivatives testing their anti-AChE inhibitory activity showed good results particularly for the acetylphosphoranyl derivative **8c** which showed also promising results either in *in vivo* behavioural tests or in *in silico* studies makes it a newly discovered candidate for AD therapy that can be furtherly improved in future works.

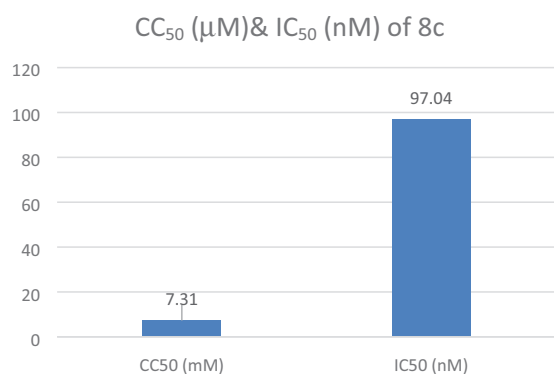


Figure 6. CC₅₀ and IC₅₀ of compound **8c**.

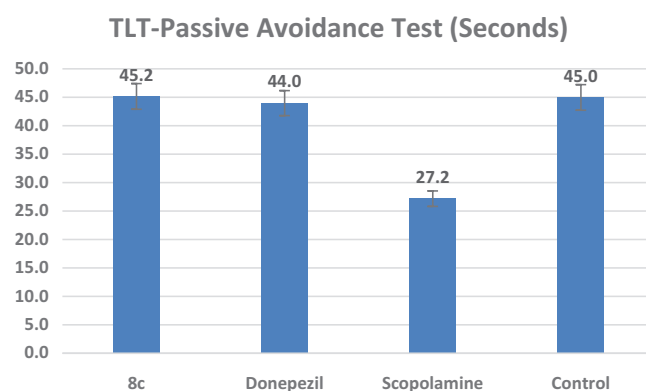


Figure 8. Effects of compound **8c** on the TLT in seconds in the step-down passive avoidance test by the scopolamine-induced cognitive impairment compared to the reference drug donepezil, the data shown are mean \pm SD ($n=5$). [#] $p < 0.01$ vs. control group.

Y-Maze Test (% Alternations)

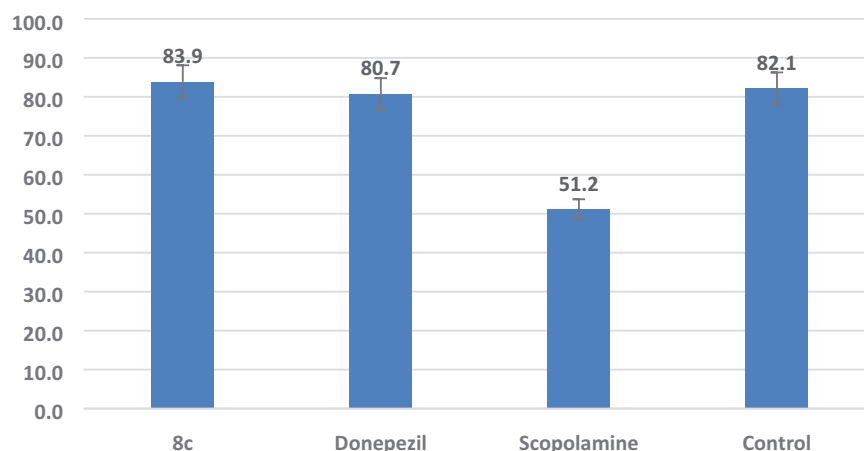


Figure 7. Effects of compound **8c** on the % of spontaneous alternations in the Y-maze test compared to the reference drug donepezil, the data shown are mean \pm SD ($n=5$). [#] $p < 0.01$ vs. control group.

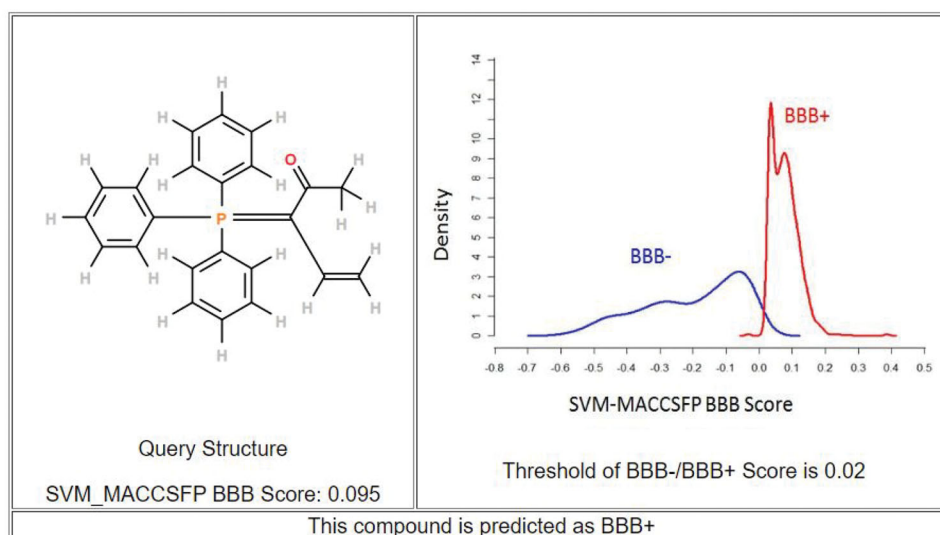


Figure 9. Prediction of BBB permeability (pkCSM webserver).

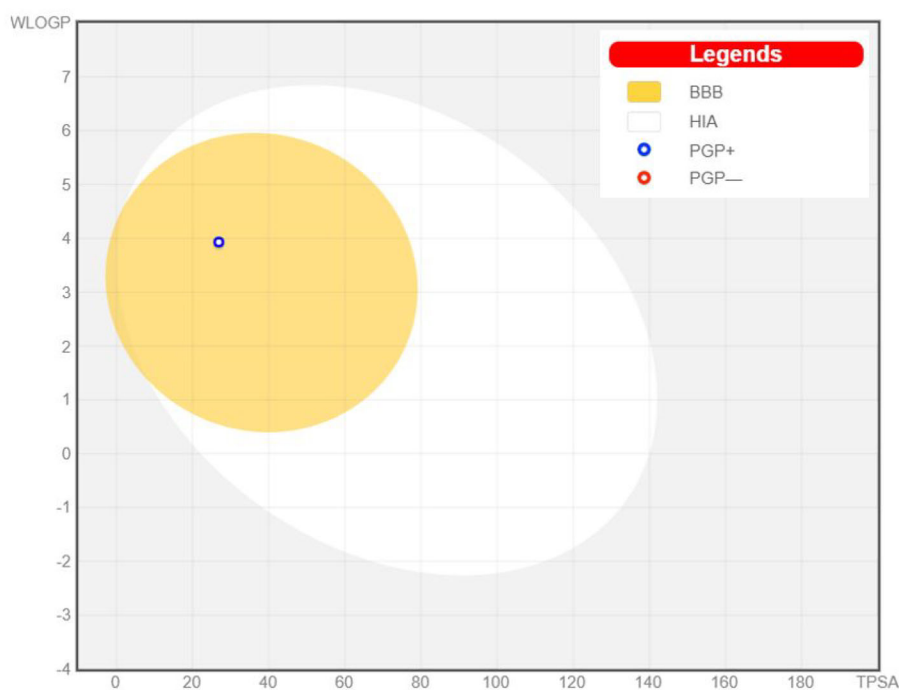


Figure 10. Prediction of BBB permeability (SwissADME webserver).

Experimental

Chemistry

Reaction of dichloro-methyl-vinyl-silane (1) with phosphacumulenes (2a) or (2b). At room temperature, dry THF (30 mL) containing 0.14 g (0.001 mol) of compound 1 and 0.001 mol of phosphacumulenes (**2a**) or (**2b**) was stirred for 6 h. For (**2a**) compound, the time was extended to 8 h while for (**2b**), the stirring was continued until no starting material was detected by TLC. Under reduced pressure, THF was distilled off and then the formed residue was purified by using silica gel with an elution system composed of pet. Ether (heated to 60–80°C)/ethyl acetate (v:v, 80:20) giving (**5a**) or (**5b**), respectively.

N-(1-chloro-1-methyl-2-(triphenylphosphoranylidene)-1H-silol-3(2H)-ylidene)aniline (5a), yellow crystals, yield 50%, mp 164 °C, IR (ν , cm^{-1}): 1573 (C=N), 1438 (C=P). ^1H NMR (500.1 MHz, CDCl_3): δ 2.01 (s, 3H, CH_3), 5.87 (d, 1H, $J_{\text{HH}} = 10$ Hz, CH), 5.95 (d, 1H, $J_{\text{HH}} = 10$ Hz, CH), 6.75–7.81 (m, 20H, arom.). ^{13}C NMR (125 MHz, CDCl_3): 16.11 (CH_3), 117.03 (CH), 120.69 (CH), 124.30, 129.13, 129.29, 129.43, 130.21, 131.88, 132.08, 132.48, 132.51, 132.68, 133.81, 135.63, 136.80 (C – aromatics), 148.00 (C=P), 151.31 (C=N). ^{31}P NMR (202.4 MHz, CDCl_3): δ 17.30. MS: m/z : 484 (M^{+2}). Anal. Calcd for $\text{C}_{29}\text{H}_{25}\text{ClNPSi}$ (482.03): C, 72.26; H, 5.23; N, 2.91; P, 6.43. Found C, 72.00; H, 4.98; N, 2.68; P, 6.11.

1-Chloro-1-methyl-2-(triphenylphosphoranylidene)-1H-silol-3(2H)-one (5b), yellow crystals, yield 35%, mp 190 °C, IR (ν ,

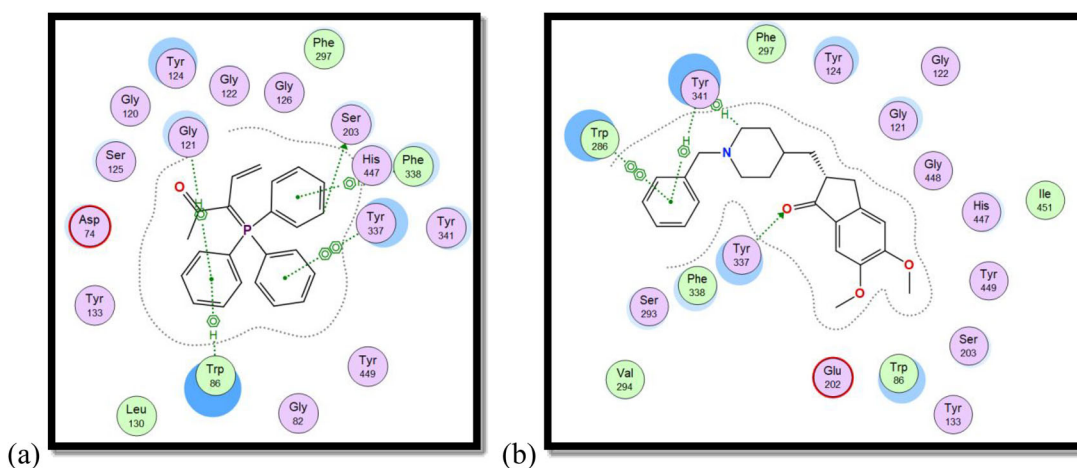


Figure 11. 2D interaction of compound **8c** (a) versus donepezil (b) with AChE active site.

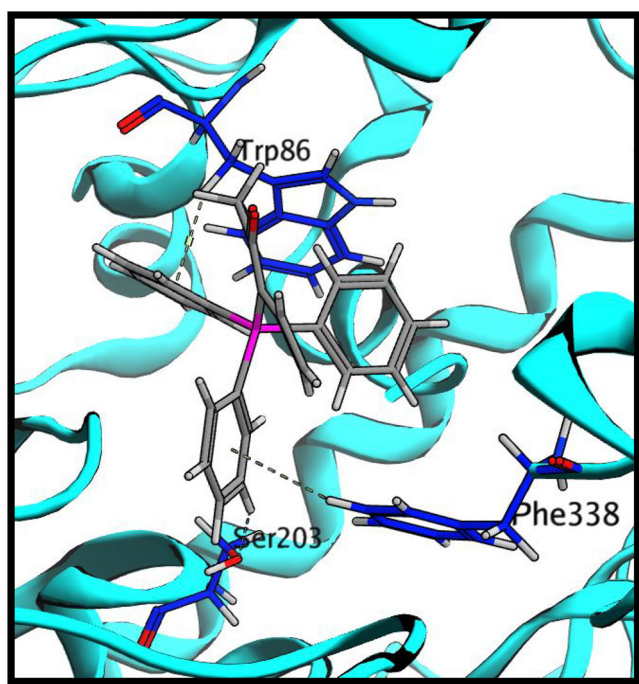


Figure 12. 3D interaction of compound **8c** with AChE active site.

cm^{-1}): 1701 (C=O), 1435 (C=P). ^1H NMR (500.1 MHz, CDCl_3): δ 1.89 (s, 3H, CH_3), 3.43 (d, 1H, $J_{\text{HH}} = 10$ Hz, CH), 6.81 (d, 1H, $J_{\text{HH}} = 10$ Hz, CH), 7.25–7.84 (m, 15H, CH aromatics). ^{13}C NMR (125 MHz, CDCl_3): 10.95 (CH_3), 117.77 (CH), 118.65 (CH), 119.78–135.31 (C-aromatics), 135.31 (C=P), 165.95 (C=O). ^{31}P NMR (202.4 MHz, CDCl_3): δ 19.40. MS: m/z : 406 (M). Anal. Calcd for $\text{C}_{23}\text{H}_{20}\text{ClO}_2\text{PSi}$ (406.92): C, 67.89; H, 4.95; P, 7.61. Found C, 67.57; H, 4.67; P, 7.39.

Reaction of dichloro-methyl-vinyl-silane (1) with stabilised phosphonium ylides (6a–6d). A solution of dichloro-methyl-vinyl-silane (**1**) (0.14 g, 0.001 mol) in dry THF (20 mL) was added to a solution of ethoxycarbonyl-(**6a**) (0.33 g, 0.001 mol) methoxycarbonyl-(**6b**) (0.34 g, 0.001 mol) acetyl-(**6c**) (0.31 g, 0.001 mol) or benzoyl-methyl-enetriphenylphosphoranes (**6d**) (0.38 g, 0.001 mol) in dry THF (20 mL). The reaction mixture was stirred for 12 h. The solvent was removed under reduced pressure and the remained residue was chromatographed on silica gel using pet. ether (60–80 °C)/ethyl acetate.

Ethyl 4-(dichloro(methyl)silyl)-2-(triphenylphosphoranylidene)butanoate (7a), was isolated by using pet. ether (60–80 °C)/ethyl acetate (v:v, 60:40) as eluent, white crystals, yield 45%, mp 137–139 °C, IR (ν , cm^{-1}): 1732 (C=O), 1438 (C=P). ^1H NMR (500.1 MHz, CDCl_3): δ 1.03 (s, 3H, CH_3), 2.51 (t, 3H, CH_2), 4.01 (t, 2H, CH_2), 5.57 (q, 2H, CH_2), 7.68–7.89 (m, 15H, aromatics). ^{13}C NMR (125 MHz, CDCl_3): 14.22 (Si- CH_3), 33.01 (CH_2 - CH_3), 63.30 (CH_2 - CH_3), 118.05 (CH_2 - CH_2), 118.93 (CH_2 - CH_2), 130.71–135.65 (C-aromatics), 165.04 (C=O). ^{31}P NMR (202.4 MHz, CDCl_3): δ 21.03. MS: m/z : (M^+ -TPPO). Anal. Calcd for $\text{C}_{25}\text{H}_{27}\text{Cl}_2\text{O}_2\text{PSi}$ (489.45): C, 61.35; H, 5.56; P, 6.33. Found C, 59.89; H, 5.48; P, 6.25.

Methyl 2-(triphenylphosphoranylidene)but-3-enoate (8b), was isolated by using pet. ether (60–80 °C)/ethyl acetate (v:v, 50:50) as eluent, white crystals, yield 65%, mp 168–170 °C, IR (ν , cm^{-1}): 1720 (C=O), 1430 (C=P). ^1H NMR (500.1 MHz, DMSO): δ 3.60 (s, 3H, OCH_3), 5.49 (d, 2H, $J_{\text{HH}} = 20$ Hz, CH_2), 7.74–8.06 (m, 16H, aromatics and CH). ^{13}C NMR (125 MHz, CDCl_3): 53.74 (CH_3), 118.05 (CH= CH_2), 119.23 (CH= CH_2), 130.49, 130.66, 134.11, 134.25, 135.51 (C-aromatics), 135.55 (C=P), 166.02 (C=O). ^{31}P NMR (202.4 MHz, CDCl_3): δ 21.02. MS: m/z : 198 (M^+ - TPP). Anal. Calcd for $\text{C}_{23}\text{H}_{21}\text{O}_2\text{P}$ (360.39): C, 76.65; H, 5.87; P, 8.59. Found C, 76.31; H, 5.50; P, 8.22.

3-(Triphenylphosphoranylidene)pent-4-en-2-one (8c), was isolated by using pet. ether (60–80 °C)/ethyl acetate (v:v, 70:30) as eluent, yellow crystals, yield 40%, mp 249–251 °C, IR (ν , cm^{-1}): 1705 (C=O), 1428 (C=P). ^1H NMR (500.1 MHz, DMSO): δ 2.36 (s, 3H, CH_3), 5.84 (d, 2H, $J_{\text{HH}} = 20$ Hz, CH_2), 7.68–7.89 (m, 16H, CH and aromatics). ^{13}C NMR (125 MHz, DMSO): 32.06 (CH_3), 118.78 (CH), 119.95 (CH_2), 130.40–135.17 (C-aromatics), 135.21 (C=P), 201.63 (C=O). ^{31}P NMR (202.4 MHz, DMSO): δ 20.67. MS: m/z : 183 (M^+ -TPP). Anal. Calcd for $\text{C}_{23}\text{H}_{21}\text{OP}$ (344.39): C, 80.21; H, 6.15; P, 8.99. Found C, 80.19; H, 6.09; P, 8.98.

1-Phenyl-2-(triphenylphosphoranylidene)but-3-en-1-one (8d), was isolated by using pet. ether (60–80 °C)/ethyl acetate (v:v, 60:40) as eluent, yellow crystals, yield 55%, mp 272–273 °C, IR (ν , cm^{-1}): 1654 (C=O), 1434 (C=P). ^1H NMR (500.1 MHz, DMSO): δ 6.44 (d, 2H, $J_{\text{HH}} = 25$ Hz, CH_2), 7.58–8.26 (m, 21H, CH aromatics and CH). ^{13}C NMR (125 MHz, DMSO): 119.07 (CH= CH_2), 120.25 (CH= CH_2), 129.40, 129.66, 130.36, 130.53, 134.09, 134.23, 135.10, 135.14, 135.35, 135.57 (C-aromatics), 135.65 (C=P), 193.10 (C=O). ^{31}P NMR (202.4 MHz, DMSO): δ 21.66. Anal. Calcd for $\text{C}_{28}\text{H}_{23}\text{OP}$ (406.46): C, 82.74; H, 5.70; P, 7.62. Found C, 82.73; H, 5.69; P, 7.60.

Reaction of (N-phenyliminovinylidene)triphenylphosphorane (2a) and/or (2-oxovinylidene)triphenylphosphorane (2b) with 1,2-diphenylethyne (10). In 20 mL toluene, compound (**2a**) (0.377 g, 1 mmol)

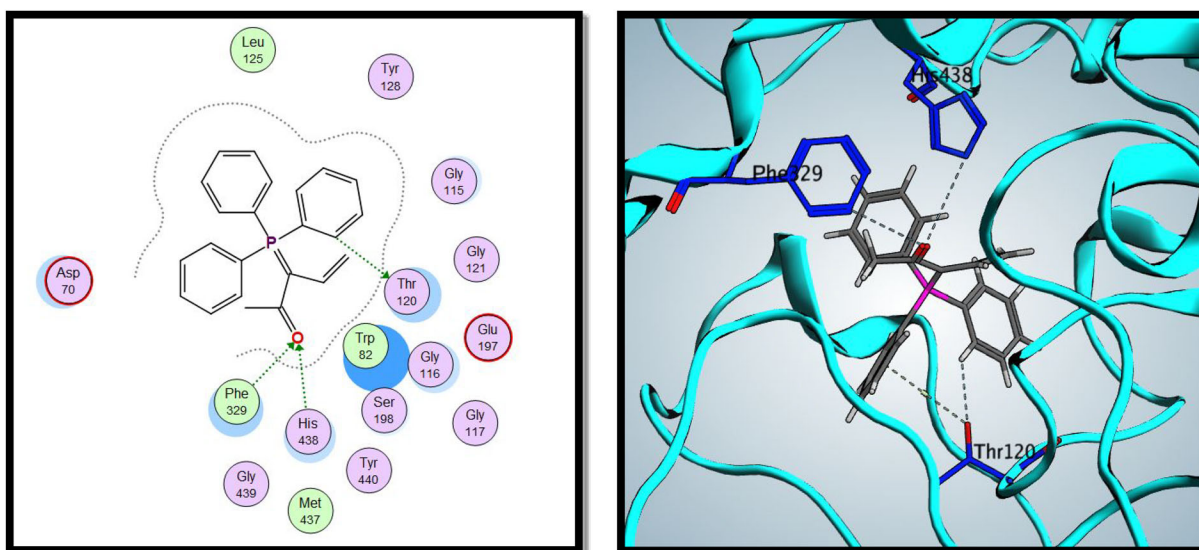


Figure 13. 2D and 3D interactions of compound **8c** with BuChE active site.

or (**2b**) (0.302 g, 1 mmol), a solution of 1,2-diphenylethyne (**10**) (0.178 g, 1 mmol) in 20 mL of toluene was added in presence of PdCl_2 . Reaction mixture was boiled for 10 h for compound and 14 h for compound (**2b**), there is a change in colour from yellow to dark brown. The reaction progress was followed by TLC, toluene was distilled under reduced pressure and then the formed residue was purified on silica gel by using an elution system of petroleum ether (60–80 °C): ethyl acetate (30:70, v/v) forming (**11a**) and (**11b**) were isolated, respectively.

N-(2,3-diphenyl-4-(triphenylphosphoranylidene)cyclobut-2-en-1-ylidene)aniline (11a), brown crystals, yield 40%, m.p. 2420 °C. IR (ν , cm^{-1}): 1609 (C=N). ^{31}P NMR (202.4 MHz, d_6 -DMSO, δ , ppm): 22.25. MS: m/z : 553 (M^{-2}). Anal. Calcd for $\text{C}_{40}\text{H}_{30}\text{NP}$ (555.65): C, 86.46; H, 5.44; N, 2.52; P, 5.57. Found C, 86.44; H, 5.42; N, 2.49; P, 5.38.

2,3-Diphenyl-4-(triphenylphosphoranylidene)cyclobut-2-enone (11b), brown crystals, yield 35%, m.p. 1170 °C. ^1H NMR (500.1 MHz, DMSO): δ 6.78–8.00 (m, 25H, CH aromatics). ^{31}P NMR (202.4 MHz, d_6 -DMSO, δ , ppm): 33.94. MS: m/z : 481 (M^+). Anal. Calcd for $\text{C}_{34}\text{H}_{25}\text{OP}$ (480.54): C, 84.98; H, 5.24; P, 6.45. Found C, 84.96; H, 5.20; P, 6.48.

Reaction of (N-phenyliminovinylidene)triphenylphosphorane (2a) and/or (2-oxovinylidene)triphenylphosphorane (2b) with hex-3-yne (12). A solution of (**2a**) (0.377 g, 1 mmol) or (**2b**) (0.302 g, 1 mmol) in 20 mL of toluene was added to a solution hex-3-yne (**12**) (0.082 g, 1 mmol) in 20 mL of toluene in presence of PdCl_2 . The reaction mixture was boiled for 7 h in case of **2a** and for 9 h in case of (**2b**) (the progress of the reaction was monitored by TLC). Under reduced pressure, toluene was distilled off and the residue was chromatographed using silica gel column using petroleum ether (60–80 °C): ethyl acetate (30:70, v/v) as eluent. Products (**13a**) and (**13b**) were isolated, respectively.

N-(2,3-diethyl-4-(triphenylphosphoranylidene)cyclobut-2-en-1-ylidene)aniline (13a), yellow crystals, yield 65%, m.p. 275–2770 °C. IR (ν , cm^{-1}): 1671 (C=N), 1555 (C=C). ^1H NMR (500.1 MHz, CDCl_3): δ 1.75 (t, 3H, CH_3), 2.16 (q, 2H, CH_2), 7.56–7.73 (20H, aromatics). MS: m/z : 458 (M^-). Anal. Calcd for $\text{C}_{32}\text{H}_{30}\text{NP}$ (459.56): C, 83.63; H, 6.58; N, 3.05; P, 6.74. Found C, 83.00; H, 6.61; N, 3.03; P, 6.60.

2,3-Diethyl-4-(triphenylphosphoranylidene)cyclobut-2-enone (13b), brown crystals, yield 58%, m.p. 1080 °C. ^1H NMR (500.1 MHz, CDCl_3): δ 1.23 (t, 3H, CH_3), 2.09 (q, 2H, CH_2), 7.45–7.72 (15H, aromatics). ^{31}P NMR (202.4 MHz, CDCl_3 , δ , ppm): 28.31. MS (m/z , %): 384 (M). $\text{C}_{26}\text{H}_{25}\text{OP}$ (384). Anal. Calcd for $\text{C}_{26}\text{H}_{25}\text{OP}$ (384.45): C, 81.23; H, 6.55; P, 8.06. Found C, 81.20; H, 6.50; P, 8.03.

Reaction of bis(trimethylsilyl)acetylene(14) with phosphacumulene (2b). Compound (**14**) (0.17 g, 0.001 mol) was added to phosphacumulene (**2b**) (0.001 mol) and refluxed for 4 h in 30 mL of dry toluene, this was proceeded until no more of the starting material could be detected by TLC. Toluene was distilled off under reduced pressure and the remained residue was purified on silica gel using pet. ether (60–80 °C)/ethyl acetate (v:v, 20:80) as eluent.

2,3-Bis(trimethylsilyl)-4-(triphenylphosphoranylidene)cyclobut-2-enone (15), yellow crystals, yield 50%, m.p. 115–1170 °C. IR (ν , cm^{-1}): 1729 (C=O), 1586 (C=C). ^1H NMR (500.1 MHz, CDCl_3): δ 2.02, 2.06 (d, 18H, 2 $\text{Si}(\text{CH}_3)_3$), 7.28–7.78 (m, 15H, aromatics). ^{31}P NMR (202.4 MHz, CDCl_3 , δ , ppm): 14.37. MS (m/z , %): 474 (M^{+2}). Anal. Calcd for $\text{C}_{28}\text{H}_{33}\text{OPSi}_2$ (472.71): C, 71.14; H, 7.04; P, 6.55. Found C, 70.79; H, 7.00; P, 6.60.

In vitro biological evaluation

In vitro AChE, BuChE and kinetic studies for AChE inhibition of compound **8c**

For AChE and BuChE inhibition experiments, Ellman *et al.* method's was applied with a few minor adjustments⁴³. According to the manufacturer's recommendations, the QuantiChrom™ AChE Inhibitor Screening Kit (IACE-100), Bioassays System, and the Cholinesterase (ChE) Activity Assay Kit, LifeSpan BioSciences, Inc., USA, were used to measure the inhibition of AChE and BuChE, respectively. The assay works by measuring the yellow hue that results from the reaction of 5,5'-dithiobis(2-nitrobenzoic acid) with thiocholine, which is created by the activity of AChE, at 412 nm. The relationship between product colour and enzyme activity after inhibition is established. Substrates included butyrylthiocholine iodide and acetylthiocholine iodide. The experiments were carried out using donepezil as the reference drug in the kit's supplied

buffer (pH 7.5). The AChE kinetics study used four different substrate doses between 12.5 and 100 nM, while synthetic (**8c**) compound was used in three concentrations between 15 and 45 nM. To study the mechanism of enzyme inhibition, line weaver-Burk reciprocal linear regression plots were created. The Dixon approach was used to calculate the K_i value by charting the slope of the lines from the double reciprocal Line-Weaver-Burk plot as a function of the test compound (**8c**) concentration⁵⁶.

MMP-2 inhibition assays for compound 8c

MMP-2 inhibitor screening assay kit (Fluorometric), Abcam® (ab139447) was used with different concentrations (0.1–1000 nM) of compound **8c** and imatinib as reference compound according to manufacturer's instructions. This assay kit uses a fluorescence resonance energy transfer (FRET) peptide as a generic MMP activity indicator. In the intact FRET peptide, the fluorescence of one part is quenched by another. After cleavage into two separate fragments by MMPs, the fluorescence is recovered. Its signal can be easily read by a fluorescence microplate reader at Ex/Em = 490/525 nm.

Self-induced $A\beta_{1-42}$ aggregation inhibition assay

The effectiveness of compound **8c** to prevent $A\beta_{1-42}$ aggregation was evaluated using the beta amyloid 1–42 ($A\beta_{42}$) Ligand Screening Assay Kit (Fluorometric) (K570-100), which was acquired from BioVision's, USA. The assay relies on Thioflavin T binding to an aggregated amyloid peptide's beta sheets to produce a strong fluorescent product (Ex/Em: 440/490 nm), which is abolished in the presence of an $A\beta_{1-42}$ ligand and results in a reduction in fluorescence or complete loss of fluorescence.

Sh-SY5Y neuroblastoma cell toxicity of compound 8c

On human neuroblastoma SH-SY5Y cells, compound **8c**'s cytotoxicity was assessed using the MTT colorimetric technique. The American Type Culture Collection provided the cells (Rockville, MD). In RPMI-1640 media containing 10% foetal bovine serum, the SH-SY5Y cells were incubated at 37 °C. The chemical was applied to the cells at various doses (0.39–100 M) for 48 h. The MTT colorimetric assay's described methodology was then used⁵⁷.

Behavioural studies (scopolamine-induced amnesia model)

In the current investigation, adult Swiss Albino mice (8–10 weeks old, weighing 25–30 g) from the National Research Centre were employed. For 1 week, animals were acclimated in a room with constant illumination, humidity, and temperature (22 °C ± 1 °C, 60%, and 12 h of light/dark cycle). Throughout the experiment, unlimited amounts of food and water were given. Mice were kept in open, opaque propylene cages with good ventilation and wide access to a variety of forages. The Research Ethics Committee of Cairo University gave its approval to all of the experimental methods used in both clinical and experimental studies.

Healthy mice were randomised into four groups of six mice each after a 1-week adaption period, at random, as follows: Group 1 is the control group, which received saline solution with 10% Tween 80. Groups II and III each received scopolamine, whereas Group IV received scopolamine + donepezil (Scopolamine plus compound **8c** group). One mg/kg of donepezil and one mg/kg of compound **8b** were given orally to the mice 30 min before scopolamine (3 mg/kg) was injected intraperitoneal to cause memory

impairment. Following the injection of scopolamine, the behavioural study will be examined 30 min later.

Morris water maze test

The rat is placed in a sizable circular pool as part of the MWM navigation job, and it must use a variety of signals to locate an invisible or visible platform that will allow it to exit the water. The performance of the rats might be affected by a variety of circumstances, such as their sex, the environment in which they were grown, exposure to pharmaceuticals, etc. The rats can escape the labyrinth using one of three fundamental strategies: a praxic strategy (remembering the motions necessary to go to the platform), a taxic strategy (using visual clues to get where they are going), or a spatial approach (using distal cues as points of reference to locate themselves)⁵⁸.

Y-maze test

In the Y-maze, a test of working memory, the animals' capacity for spontaneous alternation was evaluated⁴⁹. Three equally spaced horizontal arms measuring 120°, 45 cm long, and 16 cm high make up the Y-maze. Each mouse was put into one of the three arms of the maze and given free rein to wander from arm to arm. Both the number and order of arm inputs were recorded. The spontaneous alternation is derived from the following equation as a measure of memory performance: (Alternations/Total Arm Entries) – 2 × 100 = percent alternation. The student's *t*-test was used to assess the data.

Passive avoidance test

The passive avoidance test was conducted in a device that had two independent compartments split by a sliding door. There was a connection between the illuminated chamber and a dark compartment with an electrifiable grid floor, which was free of electric impulses. Each mouse was initially placed in the lit chamber so that it could become accustomed to it. The sliding door is then opened, allowing access to the enclosed, gloomy space. The door was shut once the animal had entered the chamber entirely, and it was then shocked with an electric shock lasting two seconds (24 V, 0.5 mA). The latency time to enter the dark container was measured to gauge working memory (Training trial). Twenty-four hours after the training trial, a test trial was carried out without application of the electric foot shock⁵⁰. Analysis of data were performed by using student's *t*-test.

In silico studies

In silico prediction of BBB permeability of compound 8c

Two webservers were used to predict BBB permeability of compound **8c**, pkCSM (<http://biosig.unimelb.edu.au/pkcsm/prediction>)⁵² and SwissADME (<http://www.swissadme.ch/>)⁵².

Molecular docking

In this study, molecular operating environment (MOE, 2019.0102) was operated for performing the molecular docking⁵⁹, energy minimised structures were gained by applying MMFF94x force field till RMSD gradient of 0.1 kcal·mol⁻¹Å⁻¹ was achieved. The X-ray crystallographic structures of human AChE in complex with (–)-galantamine was downloaded from PDB with the following ID; 4EY6⁵⁴, while the BuChE with PDB ID; 7AIY⁵⁵. The co-crystallized

ligand in each protein file was used to identify the essential binding features to the enzymes through a placing method named triangle matcher and London dG scoring algorithm.

Disclosure statement

No potential conflict of interest was reported by the author(s).

Funding

The author(s) reported there is no funding associated with the work featured in this article.

References

- Grabher BJ. Effects of Alzheimer disease on patients and their family. *J Nucl Med Technol.* 2018;46(4):335–340.
- Armstrong RA. What causes Alzheimer's disease? *Folia Neuropathol.* 2013;51(3):169–188.
- Nordberg A. Amyloid plaque imaging *in vivo*: current achievement and future prospects. *Eur J Nucl Med Mol Imaging.* 2008;35(S1):46–50.
- Colovic MB, Krstic DZ, Lazarevic-Pasti TD, et al. Acetylcholinesterase inhibitors: pharmacology and toxicology. *CN.* 2013;11(3):315–335.
- Pundir CS, Chauhan N. Acetylcholinesterase inhibition-based biosensors for pesticide determination: a review. *Anal Biochem.* 2012;429(1):19–31.
- Pope C, Karanth S, Liu J. Pharmacology and toxicology of cholinesterase inhibitors: uses and misuses of a common mechanism of action. *Environ Toxicol Pharmacol.* 2005;19(3):433–446.
- Fais A, Kumar A, Medda R, et al. Synthesis, molecular docking and cholinesterase inhibitory activity of hydroxylated 2-phenylbenzofuran derivatives. *Bioorg Chem.* 2019;84:302–308.
- Jang C, Yadav DK, Subedi L, et al. Identification of novel acetylcholinesterase inhibitors designed by pharmacophore-based virtual screening, molecular docking and bioassay. *Sci Rep.* 2018;8(1):14921.
- Desai AK, Grossberg GT. Rivastigmine for Alzheimer's disease. *Expert Rev Neurother.* 2005;5(5):563–580. Published online
- Prvulovic D, Hampel H, Pantel J. Galantamine for Alzheimer's disease. *Expert Opin Drug Metab Toxicol.* 2010;6(3):345–354.
- Benjamin B, Burns A. Donepezil for Alzheimer's disease. *Expert Rev Neurother.* 2007;7(10):1243–1249.
- Reid GA, Chilukuri N, Darvesh S. Butyrylcholinesterase and the cholinergic system. *Neuroscience.* 2013;234:53–68.
- Bentué-Ferrer D, Tribut O, Polard E, Allain H. Clinically significant drug interactions with cholinesterase inhibitors. *CNS Drugs.* 2003;17(13):947–963.
- Lane RM, Potkin SG, Enz A. Targeting acetylcholinesterase and butyrylcholinesterase in dementia. *Int J Neuropsychopharmacol.* 2006;9(1):101–124.
- Savini L, Gaeta A, Fattorusso C, et al. Specific targeting of acetylcholinesterase and butyrylcholinesterase recognition sites. Rational design of novel, selective, and highly potent cholinesterase inhibitors. *J Med Chem.* 2003;46(1):1–4. Published online
- Penke B, Bogár F, Fülöp L. β -amyloid and the pathomechanisms of Alzheimer's disease: a comprehensive view. *Molecules* 2017;22(10):1692. Published online
- Campora M, Francesconi V, Schenone S, et al. Journey on naphthoquinone and anthraquinone derivatives: new insights in Alzheimer's disease. *Pharmaceuticals* 2021; 14(1):33.
- Tomita T. Secretase inhibitors and modulators for Alzheimer's disease treatment. *Expert Rev Neurother.* 2009; 9(5):661–679.
- Sakono M, Zako T. Amyloid oligomers: formation and toxicity of $A\beta$ oligomers. *Febs J.* 2010;277(6):1348–1358. Published online
- Mroczo B, Groblewska M, Litman-Zawadzka A. The role of protein misfolding and tau oligomers (TauOs) in Alzheimer's disease (AD). *IJMS.* 2019;20(19):4661. Published online
- Glabe C. Intracellular mechanisms of amyloid accumulation and pathogenesis in Alzheimer's disease. *JMN.* 2001;17(2): 137–145. Published online
- Inestrosa NC, Sagal JP, Colombres M. Acetylcholinesterase interaction with Alzheimer amyloid beta. *Subcell Biochem.* 2005;38:299–317.
- Cui N, Hu M, Khalil RA. Biochemical and biological attributes of matrix metalloproteinases. *Prog Mol Biol Transl Sci.* 2017; 147:1–73.
- Wang XX, Tan MS, Yu JT, Tan L. Matrix metalloproteinases and their multiple roles in Alzheimer's disease. *Biomed Res Int.* 2014;2014:908636.
- Bajda M, Guzior N, Ignasik M, Malawska B. Multi-target-directed ligands in Alzheimer's disease treatment. *Curr Med Chem.* 2011;18(32):4949–4975
- Abd E, Maksoud MA, El-Makawy AI, Sh A-A. Antitumor activities of new iso(thio)cyanates and their nitrogen and sulphur heterocyclic phosphorus derivatives. *J Appl Pharm Sci.* 2019; 9(2):1–11.
- Hashem AI, El-Hussieny M, Abd E, et al. Chemistry of phosphorus ylides: part 45 synthesis of phosphoranylidene, thietane, azetidine and thiazinane derivatives as potent chemo preventative agents. *Phosphorus Sulfur Silicon Relat Elem.* 2018;193(1):1–9. Published online
- El-Hussieny M, Abd E, Maksoud MA, et al. ChemInform abstract: chemistry of phosphorus ylides. Part 44. Reaction of 1-trimethylsilyl-1H-imidazole with phosphorus reagents. A convenient synthesis of phosphorus silyl imidazoles. *ChemInform.* 2016;47(39):265–268.
- El-Hussieny M, Abd E, Maksoud MA, et al. Chemistry of phosphorus ylides part 42: reaction of dipyriddy ethanedione with phosphorus reagents. Cytotoxic activity of phosphanylidene-cyclobutane, oxaphosphetane, and pyridazinone. *Phosphorus Sulfur Silicon Relat Elem.* 2015;190(11):1845–1856.
- Maigali SS, El-Hussieny M, Soliman FM. Chemistry of phosphorus ylides. Part 37. The reaction of phosphonium ylides with indoles and naphthofurans. Synthesis of phosphanylidenes, pyrans, cyclobutenes, and pyridazine as antitumor agents. *J Heterocyclic Chem.* 2015;52(1):15–23.
- Maigali SS, Abd E, Maksoud MA, et al. Chemistry of phosphorus ylides: part 41 synthesis of antimicrobial agents from the reaction of aminoantipyrine, coumarin- and quinoline-carbaldehyde with phosphacumulene and phosphallene ylides. *J Chem Res.* 2014;38(12):754–761.
- Pan LF, Wang XB, Xie SS, et al. Multitarget-directed resveratrol derivatives: anti-cholinesterases, anti- β -amyloid

- aggregation and monoamine oxidase inhibition properties against Alzheimer's disease. *Med Chem Commun.* 2014;5(5):609–616. Published online
33. Morris JC, Cyrus PA, Orazem J, et al. Metrifonate benefits cognitive, behavioral, and global function in patients with Alzheimer's disease. *Neurology.* 1998;50(5):1222–1230. Published online
 34. López-Arrieta J, Schneider L, Cochrane Dementia and Cognitive Improvement Group. Metrifonate for Alzheimer's disease. *Cochrane Database Syst Rev.* 2006;(2):CD003155.
 35. Fujii S, Hashimoto Y. Progress in the medicinal chemistry of silicon: C/Si exchange and beyond. *Future Med Chem.* 2017;9(5):485–505.
 36. Brook MA. Silicon in organic, organometallic, and polymer chemistry. Vol. 38. New York: Wiley; 2001.
 37. Bikzhanova GA, Touloukhanova IS, Gately S, West R. Novel silicon-containing drugs derived from the indomethacin scaffold: synthesis, characterization and evaluation of biological activity. *Silicon Chem.* 2007;3(3–4):209–217. Published online
 38. Daud A, Valkov N, Centeno B, et al. Phase II trial of karenitecin in patients with malignant melanoma: Clinical and translational study. *Clin Cancer Res.* 2005;11(8):3009–3016. Published online
 39. Ramesh R, Reddy DS. Quest for novel chemical entities through incorporation of silicon in drug scaffolds. *J Med Chem.* 2018;61(9):3779–3798.
 40. El-Sayed NF, El-Hussieny M, Ewies EF, et al. New phosphazine and phosphazide derivatives as multifunctional ligands targeting acetylcholinesterase and β -Amyloid aggregation for treatment of Alzheimer's disease. *Bioorg Chem.* 2020;95:103499.
 41. Dilman AD, Ioffe SL. Carbon-carbon bond forming reactions mediated by Silicon Lewis acids. *Chem Rev.* 2003;103(3):733–772.
 42. Tripp CP, Hair ML. Reaction of methylsilanols with hydrated silica surfaces: the hydrolysis of trichloro-, dichloro-, and monochloromethylsilanes and the effects of curing. *Langmuir.* 1995;11(1):149–155.
 43. Ellman GL, Courtney KD, Andres V, Featherstone RM. A new and rapid colorimetric determination of acetylcholinesterase activity. *Biochem Pharmacol.* 1961;7:88–95.
 44. Lim NK-H, Villemagne VL, Soon CPW, et al. Investigation of matrix metalloproteinases, MMP-2 and MMP-9, in plasma reveals a decrease of MMP-2 in Alzheimer's disease. *J Alzheimers Dis.* 2011;26(4):779–786. Published online
 45. Wang H, Huang L, Wu L, et al. The MMP-2/TIMP-2 system in Alzheimer disease. *CNS Neurol Disord Drug Targets.* 2020;19(6):402–416.
 46. Ciccone L, Vandooren J, Nencetti S, Orlandini E. Natural marine and terrestrial compounds as modulators of matrix metalloproteinases-2 (MMP-2) and MMP-9 in Alzheimer's disease. *Pharmaceuticals.* 2021;14(2):86. Published online
 47. Klinkenberg I, Blokland A. The validity of scopolamine as a pharmacological model for cognitive impairment: a review of animal behavioral studies. *Neurosci Biobehav Rev.* 2010;34(8):1307–1350.
 48. Lalonde R. The neurobiological basis of spontaneous alternation. *Neurosci Biobehav Rev.* 2002;26(1):91–104.
 49. Bohdanecký Z, Jarvik ME. Impairment of one-trial passive avoidance learning in mice by scopolamine, scopolamine methylbromide, and physostigmine. *Neuropharmacol* 1967;6(3):217–222.
 50. Alavijeh MS, Chishty M, Qaiser MZ, Palmer AM. Drug metabolism and pharmacokinetics, the blood-brain barrier, and central nervous system drug discovery. *Neurotherapeutics* 2005;2(4):554–571. Published online
 51. Pires DEV, Blundell TL, Ascher DB. pkCSM: Predicting small-molecule pharmacokinetic and toxicity properties using graph-based signatures. *J Med Chem.* 2015;58(9):4066–4072
 52. Daina A, Michielin O, Zoete V. SwissADME: a free web tool to evaluate pharmacokinetics, drug-likeness and medicinal chemistry friendliness of small molecules. *Sci Rep.* 2017;7(1):42717.
 53. Cheung J, Rudolph MJ, Burshteyn F, et al. Structures of human acetylcholinesterase in complex with pharmacologically important ligands. *J Med Chem.* 2012;55(22):10282–10286.
 54. Viayna E, Coquelle N, Cieslikiewicz-Bouet M, et al. Discovery of a potent dual inhibitor of acetylcholinesterase and butyrylcholinesterase with antioxidant activity that alleviates Alzheimer-like pathology in old APP/PS1 mice. *J Med Chem.* 2021;64(1):812–839.
 55. Kuzu B, Tan M, Taslimi P, et al. Mono- or di-substituted imidazole derivatives for inhibition of acetylcholine and butyrylcholine esterases. *Bioorg Chem.* 2019;86:187–196.
 56. Kakkar T, Boxenbaum H, Mayersohn M. Estimation of K(i) in a competitive enzyme-inhibition model: comparisons among three methods of data analysis. *Drug Metab Dispos.* 1999;27(6):756–762.
 57. Edmondson JM, Armstrong LS, Martinez AO. A rapid and simple MTT-based spectrophotometric assay for determining drug sensitivity in monolayer cultures. *J Tissue Cult Methods.* 1988;11(1):15–17.
 58. Nunez J. Morris water maze experiment. *JoVE.* 2008;(19):e897. Published online
 59. Vilar S, Cozza G, Moro S. Medicinal chemistry and the molecular operating environment (MOE): application of QSAR and molecular docking to drug discovery. *Curr Top Med Chem.* 2008;8(18):1555–1572.